

Compact stars in a SU(3) Quark-Meson Model

Andreas Zacchi,¹ Rainer Stiele,^{1,2} and Jürgen Schaffner-Bielich¹

¹*Institut für Theoretische Physik, Goethe Universität,
Max-von-Laue-Straße 1, D-60438 Frankfurt, Germany*

²*Institut für Theoretische Physik, Universität Heidelberg,
Philosophenweg 16, D-69120 Heidelberg, Germany*

(Dated: June 21, 2021)

The recent observations of the massive pulsars PSR J1614-2230 and of PSR J0348+0432 with about two solar masses imply strong constraints on the properties of dense matter in the core of compact stars. Effective models of QCD aiming to describe neutron star matter can thereby be considerably constrained. In this context, a chiral quark-meson model based on a SU(3) linear σ -model with a vacuum pressure and vector meson exchange is discussed in this work. The impact of its various terms and parameters on the equation of state and the maximum mass of compact stars are delineated to check whether pure quark stars with two solar masses are feasible within this approach. Large vector meson coupling constant and a small vacuum pressure allow for maximum masses of two or more solar masses. However, pure quark stars made of absolutely stable strange quark matter, so called strange stars, turn out to be restricted to a quite small parameter range.

I. INTRODUCTION

The core of a massive star which has exhausted its thermonuclear fuel collapses in a supernova which is one of the most extreme events known to occur in the universe. The relic in the aftermath of such a cataclysmic event constitutes also one of the most extreme objects known to exist in the universe. Being more massive than our sun, but only around 20 to 30 kilometers in diameter, these so called neutron stars harbor the densest material known at present. The density in the core of such an object can even exceed nuclear density ($\rho_0 \approx 2.5 \cdot 10^{14}$ g/cm³).

For many decades it has been speculated that the material in the core of neutron stars might consist of quark matter [1, 2]. Neutron stars, or better compact stars, with a core consisting of quark matter are dubbed hybrid stars. Compact stars which are entirely made of quark matter, besides maybe a small layer of a crust of nuclei, are so called strange stars [3, 4]. Strange stars can only be realized in nature if strange quark matter is absolutely stable, i.e. the true ground state of matter [5, 6]. Hybrid stars as well as strange stars have been usually modeled by using the MIT bag model, see [7] for a review, also with corrections from hard-dense-loop calculations [8]. The Nambu-Jona-Lasinio (NJL) model has been adopted for describing quark matter in compact stars by using scalar meson fields only in [9, 10]. Vector meson fields have been added within the NJL-model in [11] showing that their contribution can substantially increase the maximum mass of a compact star with quark matter. Effects from color-superconductivity have been also considered for the properties of compact stars within NJL-type models, see [12] for a review. We point out that it was well known that hybrid stars can be as massive as two solar masses in various approaches [13, 14] and could even masquerade as neutron stars [15].

The recent measurements of the masses of the pulsars PSR J1614-2230 [16] and of PSR J0348+0432 [17] with

$M = 2.01 \pm 0.04M_\odot$ impose considerable constraints on the equation of state (EoS) for compact stars. Pure quark stars based on the simple MIT bag model could be ruled out on the basis of this measurement unless additional terms from an effective one-gluon exchange or from color-superconductivity are incorporated [18, 19]. However, the MIT bag model fails in describing QCD lattice data at nonvanishing temperature questioning its applicability for describing dense quark matter [20]. Effective models of QCD based on chiral symmetry are able to describe the lattice data at nonvanishing temperatures, as the Polyakov-loop extended versions of the NJL-model [21] or the Polyakov-loop quark-meson (PQM) model [22–24]. NJL-type models for hybrid stars have been investigated for being compatible with a maximum mass of compact stars of at least two solar masses by several groups [25–33]. Recently, the connection between NJL-type models, the Schwinger-Dyson approach and an extended version of the MIT bag model with vector-like interaction terms has been pointed out in [34–36] for modeling compact star matter incorporating features of QCD. To our knowledge, the quark-meson model has not been used to investigate the properties of hybrid stars or quark stars so far, in particular not in view of the now well established two solar mass limit for compact stars.

In this work, a modified linear- σ -model is used to describe compact star matter consisting of quark matter only. The linear σ -model is well suited to consider the chiral symmetry breaking patterns of strong interactions [37]. The quark-quark interaction is mediated by the exchange of meson fields. These interactions are conceptually different from the NJL model which considers point coupling terms between quarks. We consider scalar- and vector meson contributions to effectively model the attractive and repulsive character of the strong interaction. The maximum masses of pure quark stars are calculated by solving the Tolman-Oppenheimer-Volkoff (TOV) equations for different choices of the parameters of the quark-meson model. We further investigate the

parameter space required for the existence of absolutely stable strange quark matter and strange stars and confront these results with the new maximum mass limit for compact stars. This model has been studied in [38] for the properties of quark matter under the conditions present in core-collapse supernovae. However, the two solar mass constraint has not been investigated so far.

II. THE CHIRAL QUARK-MESON MODEL

The quark-meson model is based on the linear σ -model as discussed in detail in [37, 39] and couples mesons and quarks by utilizing chiral symmetry. The mesonic contribution in this model is given by

$$\begin{aligned} \mathcal{L}_M = & \text{tr}(\partial_\mu \varphi)^\dagger (\partial^\mu \varphi) + \text{tr}(\partial_\mu V)^\dagger (\partial^\mu V) \\ & - \lambda_1 [\text{tr}(\varphi^\dagger \varphi)]^2 - \lambda_2 \text{tr}(\varphi^\dagger \varphi)^2 \\ & - m_0^2 (\text{tr}(\varphi^\dagger \varphi)) - m_v^2 (\text{tr}(V^\dagger V)) \\ & - \text{tr}[\hat{H}(\varphi + \varphi^\dagger)] + c (\det(\varphi^\dagger) + \det(\varphi)) \end{aligned} \quad (1)$$

for $SU(3) \times SU(3)$ chiral symmetry incorporating the scalar (φ) and vector (V_μ) meson nonet. Here, m_v stands for the vacuum mass of the vector mesons and λ_1 , λ_2 , m_0 , and c are the standard parameters of the linear σ model to be fixed below. The matrix \hat{H} describes the explicit breaking of chiral symmetry. The quarks couple to the meson fields via Yukawa-type interaction terms

$$\mathcal{L}_Q = \bar{\Psi} (i\not{\partial} - g_\varphi \varphi - g_v \gamma^\mu V_\mu) \Psi \quad (2)$$

with the couplings strengths g_φ and g_v for scalar and vector mesons, respectively. Both contributions are forming the $SU(3)$ Lagrangian $\mathcal{L} = \mathcal{L}_M + \mathcal{L}_Q$ of the chiral quark-meson model.

In the mean-field approximation, the matrix φ consists of just the scalar nonstrange field σ_n and the strange field σ_s :

$$\varphi = \frac{1}{\sqrt{2}} \begin{pmatrix} \frac{\sigma_n}{\sqrt{2}} & 0 & 0 \\ 0 & \frac{\sigma_n}{\sqrt{2}} & 0 \\ 0 & 0 & \sigma_s \end{pmatrix} \quad (3)$$

and the vector fields are described by

$$V = \frac{1}{\sqrt{2}} \begin{pmatrix} \frac{\omega + \rho}{\sqrt{2}} & 0 & 0 \\ 0 & \frac{\omega - \rho}{\sqrt{2}} & 0 \\ 0 & 0 & \phi \end{pmatrix} \quad (4)$$

where ρ stands for the zeroth component of the isovector vector field, ω for the nonstrange vector field and ϕ for the strange vector field, assuming ideal mixing. Note that the spatial components of V_μ vanish in the mean-field approximation in the static case to be considered here[40]. The Lagrangian for the quark fields then reads:

$$\begin{aligned} \mathcal{L}_{F_{n,s}} = & \bar{\Psi}_n (i\not{\partial} - g_\omega \gamma^0 \omega - g_\rho \vec{\tau} \gamma^0 \rho - g_n \sigma_n) \Psi_n \\ & + \bar{\Psi}_s (i\not{\partial} - g_s \sigma_s - g_\phi \gamma^0 \phi) \Psi_s \end{aligned} \quad (5)$$

The indices n and s denote the nonstrange and strange quark contributions. The quark fields couple to the scalar- and vector meson fields σ_n , σ_s , ω , ρ , and ϕ with the respective coupling strength g_i , which are related by $SU(3)$ flavor symmetry to one overall coupling constant for the scalar meson g_φ and to another one for the vector coupling constant g_v .

Considering stationary fields in mean field approximation, the derivative terms in \mathcal{L}_M vanish and the Lagrangian is given by

$$\begin{aligned} \mathcal{L} = & \mathcal{L}_M + \mathcal{L}_Q \\ = & \frac{1}{2} (m_\omega^2 \omega^2 + m_\rho^2 \rho^2 + m_\phi^2 \phi^2) \\ & - \frac{\lambda_1}{4} (\sigma_n^2 + \sigma_s^2)^2 - \frac{\lambda_2}{4} (\sigma_n^4 + \sigma_s^4) \\ & - \frac{m_0^2}{2} (\sigma_n^2 + \sigma_s^2) + \sqrt{2} \sigma_n^2 \sigma_s c + h_n \sigma_n + h_s \sigma_s - B \\ & + \bar{\Psi}_n (i\not{\partial} - g_\omega \gamma^0 \omega - g_\rho \vec{\tau} \gamma^0 \rho - g_n \sigma_n) \Psi_n \\ & + \bar{\Psi}_s (i\not{\partial} - g_s \sigma_s - g_\phi \gamma^0 \phi) \Psi_s \end{aligned} \quad (6)$$

Here, a vacuum energy term B has been introduced in addition, see the discussion in [8, 41, 42]. The electrons will be treated as a free noninteracting Fermi-gas. The potential of the Lagrangian (6) then reads

$$\begin{aligned} \mathcal{V} = & -\frac{1}{2} (m_\omega^2 \omega^2 + m_\rho^2 \rho^2 + m_\phi^2 \phi^2) \\ & + \frac{\lambda_1}{4} (\sigma_n^2 + \sigma_s^2)^2 + \frac{\lambda_2}{4} (\sigma_n^4 + \sigma_s^4) \\ & + \frac{m_0^2}{2} (\sigma_n^2 + \sigma_s^2) - \frac{2\sigma_n^2 \sigma_s}{\sqrt{2}} \cdot c - h_n \sigma_n - h_s \sigma_s + B \end{aligned} \quad (7)$$

for the meson fields.

III. THE EQUATION OF STATE

The grand canonical potential is related to the partition function via

$$\Omega = -\frac{\ln \mathcal{Z}}{\beta} = -p. \quad (8)$$

The partition function \mathcal{Z} can be computed by a Feynman path integral over the quark fields. Performing the integration in mean field approximation, the classical stationary mesonic background fields can be replaced by their non-vanishing vacuum expectation values:

$$\mathcal{Z} = \int \prod_a \mathcal{D}\sigma_a \mathcal{D}\pi_a \int \mathcal{D}\bar{\Psi} \mathcal{D}\Psi e^{(\int_0^\beta d\tau \int_V d^3\vec{r} (\mathcal{L} + \bar{\Psi} \gamma^0 \mu \Psi))} \quad (9)$$

and one arrives at

$$\Omega = \mathcal{V} - \frac{3}{\pi^2 \beta} \int_0^\infty k^2 dk \cdot \mathcal{M} \quad (10)$$

where \mathcal{V} is the potential given in eq. (7) and the shorthand notation for \mathcal{M} is

$$\begin{aligned} \mathcal{M} = & \ln \left(1 + e^{\frac{-E_u + \mu_u - g_\omega \omega - g_\rho \rho}{T}} \right) + \ln \left(1 + e^{\frac{-E_u - \mu_u + g_\omega \omega + g_\rho \rho}{T}} \right) \\ & + \ln \left(1 + e^{\frac{-E_d + \mu_d - g_\omega \omega + g_\rho \rho}{T}} \right) + \ln \left(1 + e^{\frac{-E_d - \mu_d + g_\omega \omega - g_\rho \rho}{T}} \right) \\ & + \ln \left(1 + e^{\frac{-E_s + \mu_s - g_\phi \phi}{T}} \right) + \ln \left(1 + e^{\frac{-E_s - \mu_s + g_\phi \phi}{T}} \right) \end{aligned} \quad (11)$$

where the flavor dependent energy is

$$E_f = \sqrt{k_f^2 + (g_f \sigma_f)^2} \quad (12)$$

Compact star matter can be treated in the zero temperature limit $T \rightarrow 0$. The equations of motion of the five meson fields are given by minimizing the thermodynamic potential:

$$\frac{\partial \Omega}{\partial \sigma_n} = \frac{\partial \Omega}{\partial \sigma_s} = \frac{\partial \Omega}{\partial \omega} = \frac{\partial \Omega}{\partial \rho} = \frac{\partial \Omega}{\partial \phi} \stackrel{!}{=} 0 \quad (13)$$

For the scalar mesons one finds the gap-equations

$$\begin{aligned} \frac{\partial \Omega}{\partial \sigma_n} = & \lambda_1 \sigma_n (\sigma_n^2 + \sigma_s^2) + \frac{\lambda_2}{2} \sigma_n^3 + m_{\sigma_n}^2 \sigma_n - h_n \quad (14) \\ & + \frac{3g_n^2 \sigma_n}{\pi^2} \left(\int_0^{k_F^u} \frac{dk \cdot k^2}{E_u} + \int_0^{k_F^d} \frac{dk \cdot k^2}{E_d} \right) = 0 \end{aligned}$$

and

$$\begin{aligned} \frac{\partial \Omega}{\partial \sigma_s} = & \lambda_1 \sigma_s (\sigma_n^2 + \sigma_s^2) + \lambda_2 \sigma_s^3 + m_{\sigma_s}^2 \sigma_s - h_s \quad (15) \\ & + \frac{3g_s^2 \sigma_s}{\pi^2} \int_0^{k_F^s} \frac{dk \cdot k^2}{E_s} = 0 \end{aligned}$$

and for the vector fields

$$\frac{\partial \Omega}{\partial \omega} = -m_\omega^2 \omega + \frac{3g_\omega}{\pi^2} \left(\int_0^{k_F^u} dk \cdot k^2 + \int_0^{k_F^d} dk \cdot k^2 \right) = 0 \quad (16)$$

$$\frac{\partial \Omega}{\partial \rho} = -m_\rho^2 \rho + \frac{3g_\rho}{\pi^2} \left(\int_0^{k_F^u} dk \cdot k^2 - \int_0^{k_F^d} dk \cdot k^2 \right) = 0 \quad (17)$$

$$\frac{\partial \Omega}{\partial \phi} = -m_\phi^2 \phi + \frac{3g_\phi}{\pi^2} \int_0^{k_F^s} dk \cdot k^2 = 0 \quad (18)$$

and the respective Fermi momenta are

$$k_u = \sqrt{\left(\mu_q - \frac{2\mu_e}{3} - g_\omega \omega - g_\rho \rho \right)^2 - (g_n \sigma_n)^2} \quad (19)$$

$$k_d = \sqrt{\left(\mu_q + \frac{\mu_e}{3} - g_\omega \omega + g_\rho \rho \right)^2 - (g_n \sigma_n)^2} \quad (20)$$

$$k_s = \sqrt{\left(\mu_q + \frac{\mu_e}{3} - g_\phi \phi \right)^2 - (g_s \sigma_s)^2} \quad (21)$$

to guarantee charge neutrality through the electron chemical potential μ_e . Note that the source terms for the vector fields are given by the vector number densities,

the isovector number densities and the strange number densities due to SU(3) flavor symmetry.

The coupled equations of motion of the meson fields have to be solved self-consistently. Using eq. (8) and the relation

$$\epsilon = \Omega - \sum_i \mu_i n_i \quad (22)$$

the resulting field values then determine the EoS, which serves as an input to solve the TOV-equations:

$$\frac{dm}{dr} = \frac{4\pi r^2 \epsilon(r)}{c^2} \quad (23)$$

$$\begin{aligned} \frac{dp}{dr} = & -\frac{G\epsilon(r)m(r)}{(cr)^2} \quad (24) \\ & \times \left(1 + \frac{\rho(r)}{\epsilon(r)} \right) \left(1 + \frac{4\pi r^3 p(r)}{m(r)c^2} \right) \left(1 - \frac{2Gm(r)}{c^2 r} \right)^{-1} \end{aligned} \quad (25)$$

for the mass radius relation of compact stars.

A. Parameter range

Within the mean field approximation the mesonic fields will be treated as classical background fields. In the vacuum they will be replaced by their vacuum expectation values (VEV). In the scalar sector they are determined by the weak decay constants

$$\langle \sigma_n \rangle = f_\pi = 92.4 \text{ MeV} \quad (26)$$

$$\langle \sigma_s \rangle = \frac{2f_K - f_\pi}{\sqrt{2}} = 94.47 \text{ MeV} \quad (27)$$

with $f_K = 159.8/\sqrt{2}$ MeV. The model incorporates four free parameters. The constituent quark mass will be varied in a range around $m_q = 100$ MeV to 400 MeV. It determines the scalar coupling for the nonstrange (28) and strange (29) condensates via the Goldberger-Treiman relation

$$g_{u,d} = g_n = \frac{m_q}{f_\pi} \quad (28)$$

and from SU(3) symmetry

$$g_s = g_n \cdot \sqrt{2}. \quad (29)$$

The vector coupling is independent on the constituent quark mass, it will be varied in a scale similar to the one of the scalar coupling, $g_\omega \sim g_n$, to study its influences in an appropriate range [38]. The coupling constant of the ϕ -meson is fixed again by SU(3) symmetry:

$$g_\omega = g_\rho = \frac{g_\phi}{\sqrt{2}} \quad (30)$$

To fix the remaining parameters of the scalar mesons, the following masses have been adopted:

$$m_\pi = 138 \text{ MeV} \quad (31)$$

$$m_K = 496 \text{ MeV} \quad (32)$$

$$m_\eta = 547.5 \text{ MeV} \quad (33)$$

$$m_{\eta'} = 957.78 \text{ MeV} \quad (34)$$

The experimentally not well determined mass of the σ -meson could cover a range from $m_\sigma = 400$ MeV to 1000 MeV. The explicit symmetry breaking terms are defined via the Gell-Mann-Oakes-Renner relation [37] as follows

$$h_n = f_\pi m_\pi^2 \quad (35)$$

$$h_s = \sqrt{2} f_K m_K^2 - \frac{h_n}{\sqrt{2}} \quad (36)$$

The parameter λ_1 has to be determined via the relation [37]

$$m_\sigma^2(m^2, \lambda_1) \leftrightarrow m_\sigma^2(m^2(\lambda_1), \lambda_1) \leftrightarrow m_\sigma^2(\lambda_1) \quad (37)$$

and λ_2 is given by

$$\lambda_2 = \frac{3m_K^2(2f_K - f_\pi) - m_\pi^2(2f_K + f_\pi)}{(3f_\pi^2 + 8f_K(f_K - f_\pi))(f_K - f_\pi)} - \frac{2(m_{\eta'}^2 + m_\eta^2)(f_K - f_\pi)}{(3f_\pi^2 + 8f_K(f_K - f_\pi))(f_K - f_\pi)} \quad (38)$$

The large mass of the η' -meson (which, as a Goldstone boson should be nearly massless, see [43, 44]) will be implemented by the axial anomaly term with the coupling strength c determined by

$$c = \frac{m_K^2 - m_\pi^2}{f_K - f_\pi} - \lambda_2 \cdot (2f_K - f_\pi). \quad (39)$$

The last free parameter is the vacuum pressure at vanishing chemical potential B , which we choose to cover a range from $B^{1/4} = 0$ MeV to 140 MeV. While varying one parameter in the following, the other parameters will be held fixed at some canonical values chosen to be $m_\sigma = 600$ MeV, $m_q = 300$ MeV, $g_\omega = 2$ and $B^{1/4} = 120$ MeV.

IV. RESULTS

A. Variation of the vector coupling constant g_ω

The vector coupling models the repulsive character of the strong interaction. Analogue to the scalar coupling, which is dependent on the constituent quark mass, the vector coupling will be changed in a range from $g_\omega = 1$ to 7.

Figure 1 shows the nonstrange scalar condensates for various values of g_ω . There is a crossover for values of $g_\omega \gtrsim 4$. For values of $g_\omega \lesssim 4$ there is a jump in the scalar condensate, which is present at smaller chemical potential μ_q for smaller values of g_ω . The chiral transition for $g_\omega = 2.0$ takes place at $\mu \sim 325$ MeV. Because of explicit symmetry breaking, the condensate does not vanish entirely in the chirally restored phase, see e.g. the discussion in [37].

Note that the jump is also visible for the strange condensate, which can be seen in Fig. 2. Because of the larger mass of the strange quark the jump is not that

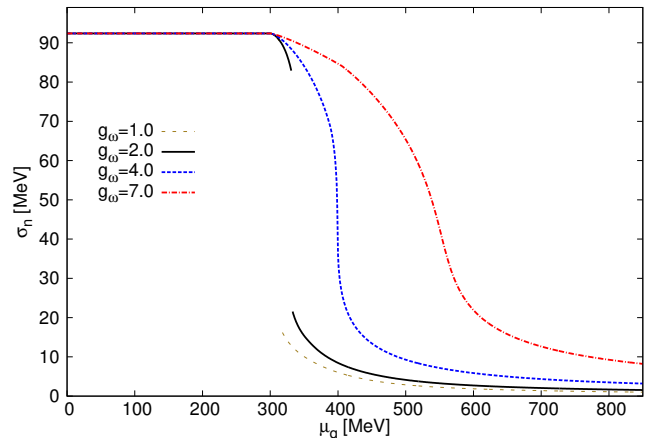


FIG. 1. The nonstrange scalar condensate for various values of the vector coupling constant g_ω at fixed values of $m_q = 300$ MeV, $m_\sigma = 600$ MeV and $B^{1/4} = 120$ MeV.

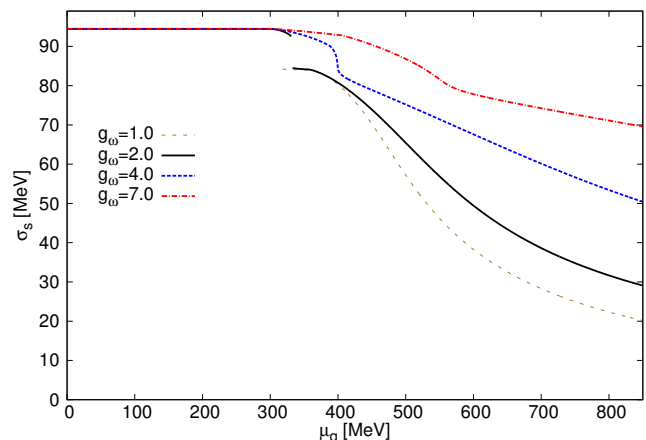


FIG. 2. The strange scalar condensates for various values of the vector coupling constant g_ω at fixed $m_q = 300$ MeV, $m_\sigma = 600$ MeV and $B^{1/4} = 120$ MeV.

pronounced and the field changes rather smoothly staying at larger values even in the chirally restored phase up to the largest considered values of the chemical potential.

An increase of the repulsive coupling g_ω provokes the scalar fields to increase too. This is due to the subtraction of the terms including the vector fields from the chemical potential μ_q in eqs. (19), (20) and (21). Larger vector field terms require larger chemical potential to compensate for their impact.

The EoS for various values g_ω is plotted in Fig. 3. For a larger value of the vector coupling constant, the repulsion between quarks increases, the slope of the EoS increases and the EoS becomes stiffer, i.e. quark matter requires more pressure to be compressed to a given energy density.

The corresponding solutions of the TOV equations can be seen in Fig. 4. With a stiffer EoS the maximum mass increases. This increase in the maximum mass is due to the repulsive character of the vector mesons which gives

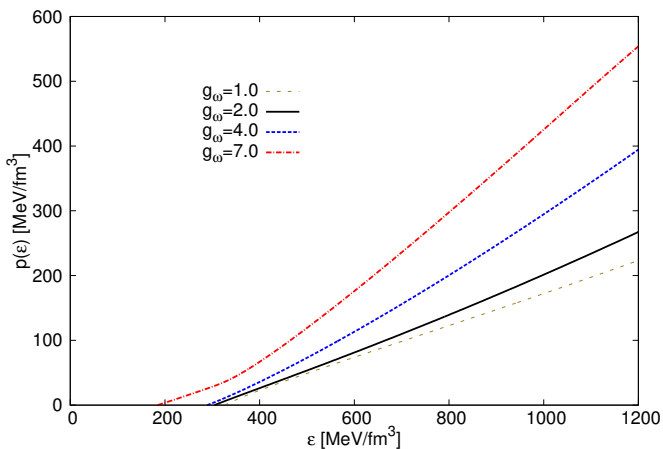


FIG. 3. The EoS for various values of the vector coupling constant g_ω at fixed $m_q = 300$ MeV, $m_\sigma = 600$ MeV and $B^{1/4} = 120$ MeV.

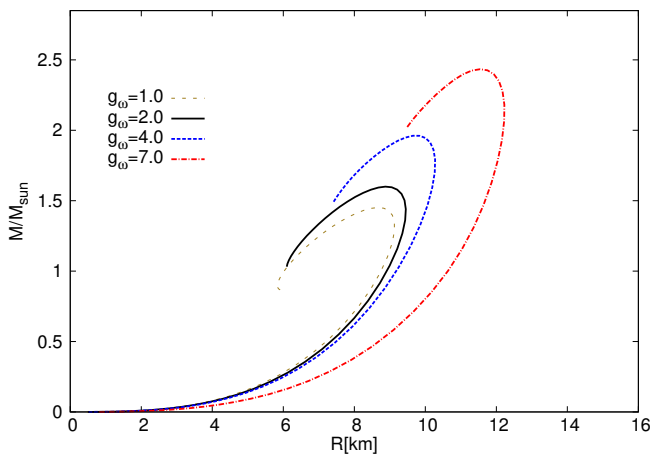


FIG. 4. The mass-radius relation for various values of the vector coupling constant g_ω at fixed $m_q = 300$ MeV, $m_\sigma = 600$ MeV and $B^{1/4} = 120$ MeV.

a higher pressure at a given energy density (see Fig. 3) and therefore quark matter is able to stabilize more mass against the pull of gravity. With the choice of $g_\omega = 4.0$ and the other parameters held fixed at $m_q = 300$ MeV, $m_\sigma = 600$ MeV and $B^{1/4} = 120$ MeV one reaches a maximum mass of $\sim 2.1M_\odot$ at a radius of 10 km. Smaller values of the vector coupling constant result in compact star configurations with a maximum mass smaller than $2M_\odot$ which is in conflict with observations. Hence, the vector-like interactions between quarks are necessary in the model used to achieve the $2M_\odot$ mass limit in a physically reasonable range of our parameters.

B. Variation of the constituent quark mass

Raising the value of the constituent quark-mass increases the scalar coupling, see equations (28) and (29).

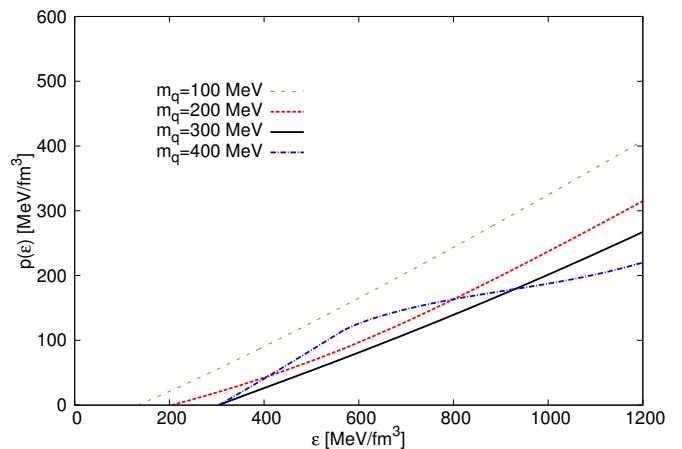


FIG. 5. The EoS while varying m_q with fixed $g_\omega = 2.0$, $m_\sigma = 600$ MeV and $B^{1/4} = 120$ MeV.

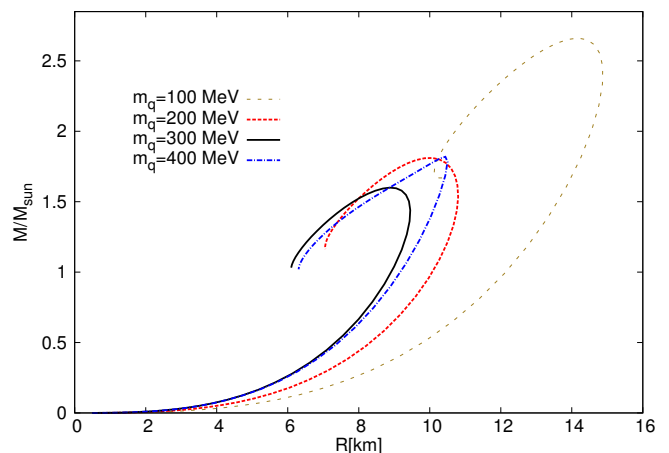


FIG. 6. The mass-radius relation for various values of m_q at fixed $g_\omega = 2.0$, $m_\sigma = 600$ MeV and $B^{1/4} = 120$ MeV

The values of the scalar condensate have been checked with the results of [39] and found to be in accordance.

We find that a crossover transition is present for values of $\mu_q \lesssim 300$ MeV, whereas for values $\mu_q \geq 300$ MeV a first order phase transition emerges, and the chiral condensate jumps. For even higher values, the strength of the first order chiral phase transition increases.

The EoS shown in Fig. 5 displays a softening for increasing values of m_q , leading to smaller maximum masses of the compact star configuration, as can be seen in Fig. 6. The trend of the curve of the EoS for $m_q \geq 300$ MeV shows a slightly different behaviour. For $m_q = 100$ MeV the $2M_\odot$ -limit is exceeded. In this case the scalar condensates would exhibit a smooth crossover-like behavior as a function of the chemical potential.

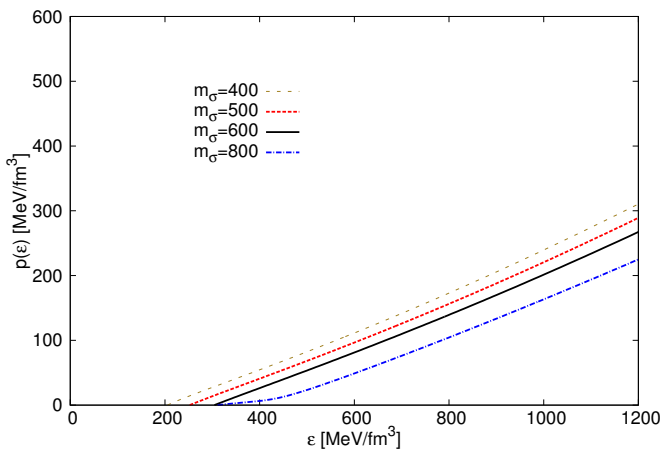


FIG. 7. The EoS for various values of m_σ at fixed $g_\omega = 2.0$, $m_q = 300$ MeV and $B^{1/4} = 120$ MeV.

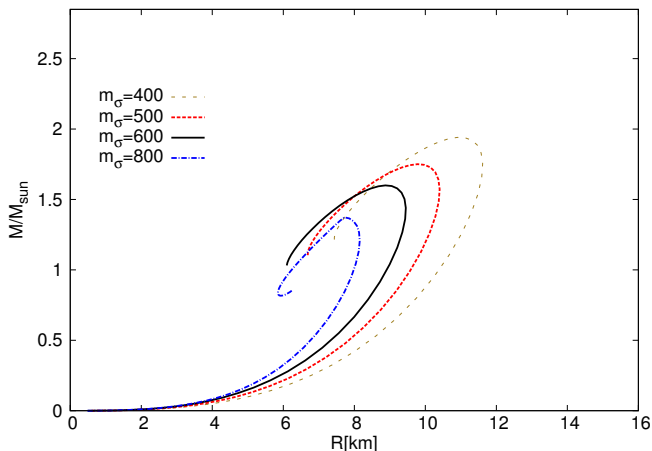


FIG. 8. The mass-radius relation for various values of m_σ at fixed $g_\omega = 2.0$, $m_q = 300$ MeV and $B^{1/4} = 120$ MeV.

C. Variation of the σ -Meson mass

We find that with increasing σ meson mass m_σ the phase transition becomes a crossover ($m_\sigma \geq 800$ MeV), whereas values of $m_\sigma \leq 800$ MeV lead to first order phase transitions at $\mu_q \simeq 300$ MeV. For $m_\sigma = 600$ MeV the first order phase transition takes place at $\mu_q \sim 330$ MeV. The behavior of the nonstrange and strange condensates is found to be similar to the discussion in section IV A.

The resulting EoS is shown in Fig. 7. The EoS softens with increasing scalar meson mass m_σ . Hence, one expects a mass-radius relation which is located at smaller values of the mass and radius for increasing the σ meson mass, which can clearly be observed in Fig. 8. So a smaller value of m_σ leads to higher maximum masses of the compact star.

The mass of the sigma meson m_σ is directly related to the parameters λ_1 and λ_2 , according to (37) and (38). These parameters are, among others in the SU(3) case,

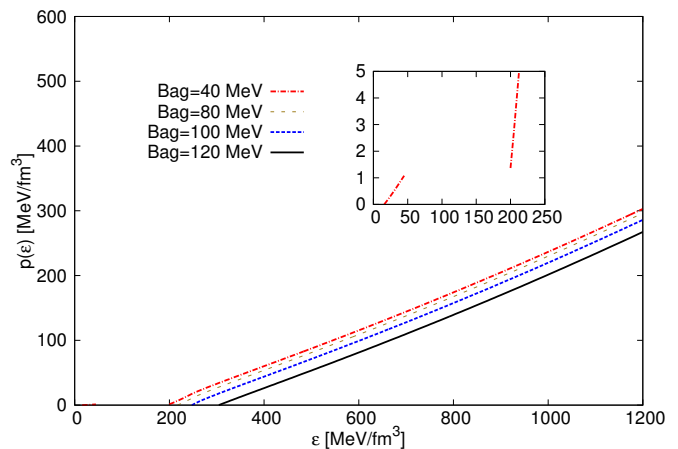


FIG. 9. The equation of state for various values of the vacuum constant $B^{1/4}$ at fixed values of $m_\sigma = 600$ MeV, $g_\omega = 2.0$ and $m_q = 300$ MeV.

mainly responsible for the potential depth for spontaneous symmetry breaking. The impact of the sigma meson mass on the chiral condensate and the EoS is nontrivial. A simple explanation might be that for a higher mass of the scalar meson more energy is needed to overcome the barrier and reach the second minimum of the potential, which leads also to a shift of the chiral phase transition to a larger chemical potential μ_q and a crossover-like behavior of the chiral condensates at high densities.

D. Variation of the vacuum constant

Figure 9 shows the equation of state for various values of the vacuum constant $B^{1/4}$. The equation of state does not change significantly when varying the vacuum constant. The vacuum constant B drops out in the equations of motion (13) so that it does not affect the values of the meson fields.

The slopes of the curves are very similar to each other. The pressure vanishes at lower energy densities for a smaller vacuum constant. Note that the curve for the vacuum constant $B^{1/4} = 40$ MeV is not simply shifted but the jump in the energy density is in this case at a small, but non-vanishing value of the pressure. This can be observed in the inlay of Fig. 9. This property leads to an additional stable branch in the mass-radius relation shown in Fig. 10. For $B^{1/4} = 40$ MeV there are two stable branches. One up to $0.6 M_\odot$ at a radius of $\simeq 19$ km and a second branch between $\simeq 14$ km and $\simeq 12$ km radius and up to a maximum mass of $\sim 2M_\odot$. These so called twin star solutions [8, 41] are beyond the scope of this article and are discussed in more detail in [8, 45–51] and in the forthcoming publication [52]. See [45] for a detailed discussion on stability.

The mass-radius relation depicted in Fig. 10 demonstrates that larger maximum masses can be achieved for

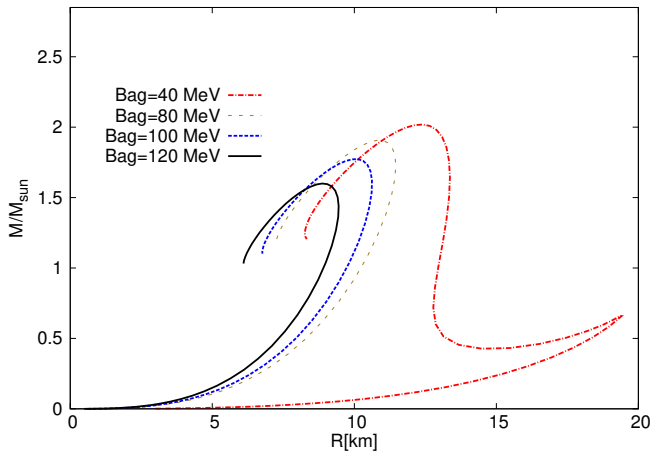


FIG. 10. The mass-radius relation for various values of the vacuum constant $B^{1/4}$ with fixed values of $m_\sigma = 600\text{MeV}$, $g_\omega = 2.0$ and $m_q = 300\text{ MeV}$. The maximum mass increases significantly for a lower value of the vacuum constant B .

smaller values of the vacuum constant B . We point out that the standard choice of the vacuum pressure in refs. [8, 41] was a value of $B^{1/4} = 120\text{ MeV}$. For this value the resulting mass-radius relation has a maximum mass around $1.6M_\odot$ at a radius of around 9 km, when fixing the other parameters of the model at their standard values. The vacuum constant has a strong influence on the mass-radius relation, and the maximum mass of a compact star can easily reach values of $2M_\odot$. Choosing $B^{1/4} = 40\text{ MeV}$ the resulting compact star configurations have a maximum mass of $\sim 2M_\odot$ at a radius of 12 km.

E. Stability considerations

The properties of quark matter have to fulfill certain conditions in order to allow for the possibility of pure quark matter stars studied above.

Normal matter, consisting of ordinary nuclei, is stable on cosmological timescales, so it does not decay to quark matter with its quark constituents of up-quarks and down-quarks. This observation requires that two flavor quark matter can not be more stable than ordinary nuclear matter, meaning that the energy per baryon has to be higher than the one of the most stable known element in nature: ^{56}Fe . We adopt a value of energy per baryon of $E/A = 930\text{ MeV}$ for nuclei and add a 4 MeV correction due to surface effects of lumps of quark matter balls as discussed in [53]. Hence the critical condition for two-flavor quark matter reads

$$\left. \frac{E}{3A} \right|_{p=0} = \left. \frac{\epsilon}{n_q} \right|_{p=0} \gtrsim 311\text{ MeV} \quad (40)$$

This condition guarantees the stability of atomic nuclei, meaning that atomic nuclei do not dissolve into their constituent quarks.

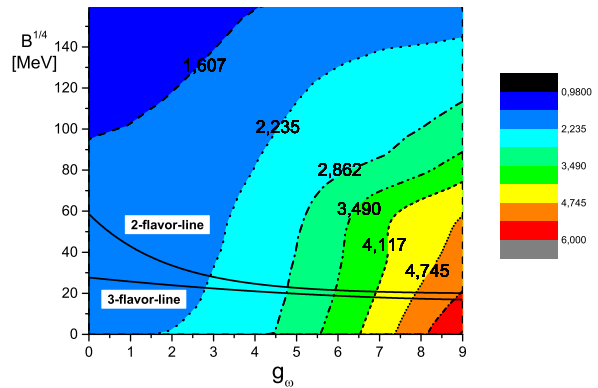


FIG. 11. Maximum masses for three-flavor pure quark stars in the plane of the vacuum constant B and the vector coupling constant g_ω . The two-flavor and three-flavor lines delineate the region for hybrid stars (above the two-flavor line) and pure quark stars (below the three-flavor line). Pure quark star configurations do not appear for the parameters chosen ($m_\sigma = 600\text{ MeV}$ and $m_q = 300\text{ MeV}$).

On the other hand three-flavor quark matter, i.e. quark matter consisting of up-, down- and strange quarks, could be more stable than ordinary nuclei which is the Bodmer-Witten hypothesis [5, 6]. Ordinary nuclear matter can not decay to strange quark matter, as there is a barrier between these two states of matter due to strangeness conversion via weak interactions with a corresponding conversion timescale much longer than the age of the universe. The presence of the new degree of freedom, the strange quark, in quark matter lowers the overall energy per baryon, so that this state could be energetically favorable compared to nuclear matter. Hence, the condition for absolutely stable strange quark matter of $E/A < 930\text{ MeV}$ can be recast in the form

$$\left. \frac{E}{3A} \right|_{p=0} = \left. \frac{\epsilon}{n_q} \right|_{p=0} \leq 310\text{ MeV} \quad (41)$$

In the following we will denote the physical condition for two-flavor quark matter, eq. (40), the two-flavor condition (or two-flavor line in the plots) and the one for three-flavor quark matter, eq. (41), the three-flavor condition (or three-flavor line in the plots).

Figures 11 and 12 depict the maximum masses in dependence of the parameters $B^{1/4}$, m_σ and g_ω . In general, smaller values of the vacuum constant B and higher values for the vector coupling constant g_ω lead to higher maximum masses.

Figure 11 shows as a contour plot the dependencies of the maximum mass of pure quark star configurations on the vacuum constant $B^{1/4}$ and the vector coupling constant g_ω . For $B^{1/4} = 120\text{ MeV}$ and $g_\omega = 2.0$ one finds a maximum mass of about $1.6M_\odot$, which can be cross-checked with Figs. 4, 6, 8 and 10.

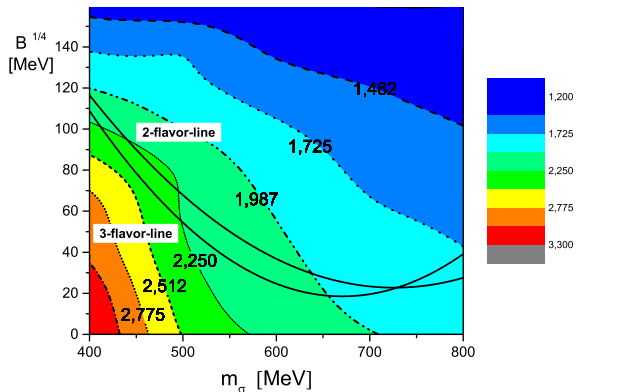


FIG. 12. Maximum masses for three-flavor pure quark stars in the plane of the vacuum constant $B^{1/4}$ and the sigma meson mass m_σ . The two-flavor and three-flavor lines delineate the region for hybrid stars (above the two-flavor line) and pure quark stars (below the three-flavor line). Pure quark star configurations are possible for a small window at large values of the sigma meson mass m_σ (here $g_\omega = 2$ and $m_q = 300$ MeV are held fixed).

The two-flavor line indicates the two-flavor constraint (40) and the three-flavor line the three-flavor constraint (41). In the area above the two-flavor line the condition (40) is fulfilled, i.e. normal matter can not decay to two-flavor quark matter as observed in nature. For a vanishing vector repulsion the vacuum constant has to be larger than $B^{1/4} > 60$ MeV in order for quark matter to obey the two-flavor constraint. The critical value for $B^{1/4}$ decreases towards $B^{1/4} = 20$ MeV with increasing vector coupling constant. Hybrid star configurations are located in the parameter range above the two-flavor line.

In the area below the three-flavor line the condition (41) is fulfilled. Within the chosen parameters the three-flavor line is nearly independent on the vector coupling constant g_ω being between $B^{1/4} \sim 28$ MeV for a vanishing vector coupling constant and $B^{1/4} \sim 20$ MeV for $g_\omega = 9.0$. The vacuum pressure dictates at which energy density ϵ_0 the pressure vanishes, which determines via the Hugenholtz-van Hove theorem the binding energy of quark matter: $E_B/A = \mu_B = \epsilon_0/n_B$. As, there is no region, where both conditions (40) and (41) are fulfilled simultaneously, no pure quark star configurations emerge in the contour plot for the chosen parameters of $m_\sigma = 600$ MeV and $m_q = 300$ MeV.

Figure 12 shows the maximum masses and the quark matter constraints (40) and (41) in the parameter plane of the vacuum constant $B^{1/4}$ and the σ -meson mass m_σ . The two-flavor line starts at $B^{1/4} = 115$ MeV for $m_\sigma = 400$ MeV, with the three-flavor line being slightly below the two-flavor line. Both lines decrease in a similar manner with increasing mass of the σ -meson. At $B^{1/4} = 26$ MeV and $m_\sigma = 725$ MeV both lines intersect and from that point on the three-flavor line is above

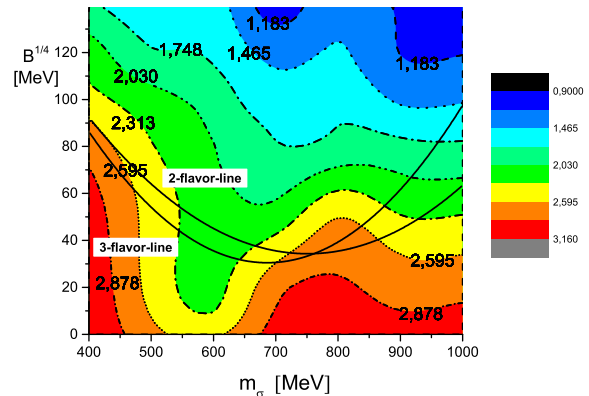


FIG. 13. Maximum masses and stability configurations for pure quark star configurations as in Fig. 12 for a slightly larger vector coupling constant of $g_\omega = 3.0$.

the two-flavor line. This means that from there on, in a small parameter space (the small area enclosed by both lines), pure quark star configurations are stable. The corresponding highest maximum mass for pure quark stars in Fig. 12 with $g_\omega = 2$ and $m_q = 300$ MeV held fixed is located at $m_\sigma \sim 725$ MeV and $B^{1/4} \sim 26$ MeV with a value of $\sim 1.8M_\odot$ which is not compatible with the recent pulsar mass measurements.

A high mass of the sigma meson seems to be necessary in order to fulfill the constraints for pure quark star configurations, i.e. equation (40) and (41), in contrast to the variation of the vector coupling constant. A projection on the g_ω - m_σ -plane on the other hand (with a fixed value of $B^{1/4} = 120$ MeV) leads to a null result for pure quark star configurations due to the high value of the vacuum constant. Only a small value of the vacuum constant leads to pure quark star configurations.

As the two solar mass limit for pure quark stars with $g_\omega = 2.0$ is not reached, we increase the repulsive vector interaction g_ω in the following to a value of $g_\omega = 3.0$. The resulting maximum masses and lines of constraints are shown in Fig. 13. There is an overall increase of the maximum mass as expected for a greater repulsive interaction. Surprisingly, for $m_\sigma \geq 600$ MeV the maximum mass increases with the σ meson mass again, which can not be seen in Fig. 12. This behavior indicates a switch in the dominance of the scalar- and vector field contributions to the stiffness of the equation of state. Above a certain value, around $g_\omega \sim 2.75$, the repulsive fields gain on their influence on the maximum masses compared to the attractive scalar fields. A combination of $g_\omega \gtrsim 2.75$ and $m_\sigma \geq 600$ MeV leads then to higher maximum masses with increasing σ meson mass instead.

The lines of the two constraints intersect at $B^{1/4} \sim 32$ MeV and $m_\sigma \sim 760$ MeV. From this point on pure quark star configurations are realized between the two lines of constraint as discussed above. Note that in

Fig. 13 results are shown for σ meson masses of up to $m_\sigma = 1000$ MeV. At the intersecting point at $B^{1/4} \sim 32$ MeV and $m_\sigma \sim 760$ MeV the maximum mass of the quark star would be $\sim 2.7M_\odot$, being smaller for larger values of the σ meson mass m_σ and larger values of the vacuum constant. A pure quark star with a maximum mass of $\sim 2.0M_\odot$ can be found at a vacuum constant of $B^{1/4} = 70$ MeV for σ meson masses between $900 \text{ MeV} \leq m_\sigma \leq 1000 \text{ MeV}$.

F. Comparison with other models

In the following we compare our findings with other approaches for studying pure quark stars, i.e. selfbound strange stars. For hybrid stars not discussed here a low-density hadronic equation of state needs to be augmented for a thorough discussion which is beyond the scope of the present investigation, but will be addressed in [52].

Coelho et al. [54] use a SU(2)-flavor symmetric NJL model with a repulsive vector coupling. For a large vector coupling their EoS stiffens like in our model calculations leading to higher masses at given radii.

Weissenborn et al. [19] use an extended quark bag model. Strange stars can reach maximum masses beyond $2M_\odot$ in their work if additional terms compared to the standard MIT bag model are introduced, either in the form of some effective interaction motivated from one-gluon exchange or from a large gap motivated from color-superconductivity. They found a maximum mass for a pure quark star to be at $2.54M_\odot$, which is in the same order of magnitude as in this work.

In the work by Torres and Menezes [55] pure quark stars would have maximum masses of $2.29M_\odot$. They use a model, where the quark masses are assumed to have a certain given density dependence causing a stiffening of the EoS compared to the standard MIT bag model.

V. SUMMARY

In this work a chiral Quark-Meson model in SU(3)-flavor symmetry has been studied for the description of compact stars consisting of pure quark matter. The thermodynamical properties have been calculated via the grand potential in the zero temperature limit. The gap equations were solved selfconsistently to determine the EoS, which serves as an input to solve the TOV equations

and compute the mass-radius relations. The EoS and the dependence on the four free parameters of the model, the vector coupling constant, the constituent quark mass, the sigma meson, and the vacuum constant, were systematically investigated.

The variation of the vector coupling constant showed the highest impact on the EoS. The higher its value, the stiffer the EoS, leading to maximum masses in excess of $2M_\odot$. The dependence of the EoS with the constituent quark mass m_q in vacuum, which fixes the scalar coupling constant, is such that the smaller m_q , the stiffer the EoS. The mass of the σ -meson studied covers a range from 400 to 1000 MeV. For a smaller mass of the σ -meson the EoS becomes stiffer. Finally, the vacuum constant does not affect the values of the meson fields, it just shifts the energy density at a given pressure. The EoS substantially stiffens when decreasing the vacuum constant so that for small values of $B^{1/4} \lesssim 40$ MeV maximum masses of up to $\geq 2M_\odot$ could easily be reached.

The stability of two-flavor and three-flavor quark matter have been checked as well, to see whether or not the model parameter space allows for physically reasonable quark matter properties in the SU(3)-flavor approach. The $2M_\odot$ limit set by the recently discovered millisecond pulsars PSR J1614-2230 [16] and PSR J0348+0432 [17] could be reached. Having considered the stability constraints in the equations (40) and (41), most choices of the parameter space were found to be hybrid stars. Nonetheless, pure quark star configurations with $\sim 2M_\odot$ can be realized in a small physically reasonable parameter range. A sizable additional repulsion mediated by the exchange of vector mesons as well as a nonvanishing vacuum pressure seems to be crucial to allow for maximum mass configurations of quark stars compatible with the recent pulsar mass measurements.

ACKNOWLEDGMENTS

We thank Margit Maly for discussions during the initial stage of this project. AZ was supported by the Friedrich-Ebert-Stiftung (FES). RS has been supported by the Heidelberg Graduate School of Fundamental Physics (HGSFP) and through the Helmholtz Graduate School for Heavy-Ion Research (HGS-HIRE) and the Graduate Program for Hadron and Ion Research (GP-HIR).

-
- [1] D. D. Ivanenko and D. F. Kurdgelaidze, *Astrophys. J.* **1**, 251 (1965).
 - [2] N. Itoh, *Prog.Theor.Phys.* **44**, 291 (1970).
 - [3] P. Haensel, J. L. Zdunik, and R. Schaeffer, *Astron. Astrophys.* **160**, 121 (1986).
 - [4] C. Alcock, E. Farhi, and A. Olinto, *Astrophys. J.* **310**, 261 (1986).
 - [5] A. R. Bodmer, *Phys. Rev. D* **4**, 1601 (1971).
 - [6] E. Witten, *Phys. Rev. D* **30**, 272 (1984).
 - [7] F. Weber, *Prog. Part. Nucl. Phys.* **54**, 193 (2005), astro-ph/0407155.
 - [8] K. Schertler, C. Greiner, P. K. Sahu, and M. H. Thoma, *Nucl. Phys.* **A637**, 451 (1998).
 - [9] K. Schertler, S. Leupold, and J. Schaffner-Bielich, *Phys.*

- Rev. C **60**, 025801 (1999), arXiv:astro-ph/9901152.
- [10] A. Steiner, M. Prakash, and J. M. Lattimer, Phys. Lett. B **486**, 239 (2000).
- [11] M. Hanauske, L. Satarov, I. Mishustin, H. Stoecker, and W. Greiner, Phys. Rev. **D64**, 043005 (2001), arXiv:astro-ph/0101267 [astro-ph].
- [12] M. Buballa, Phys.Rept. **407**, 205 (2005), arXiv:hep-ph/0402234 [hep-ph].
- [13] T. Klähn, D. Blaschke, F. Sandin, C. Fuchs, A. Faessler, H. Grigorian, G. Röpke, and J. Trümper, Phys. Lett. **B654**, 170 (2007), arXiv:nucl-th/0609067.
- [14] M. Alford, D. Blaschke, A. Drago, T. Klähn, G. Pagliara, and J. Schaffner-Bielich, Nature **445**, E7 (2006), astro-ph/0606524.
- [15] M. Alford, M. Braby, M. Paris, and S. Reddy, Astrophys.J. **629**, 969 (2005), arXiv:nucl-th/0411016 [nucl-th].
- [16] P. Demorest, T. Pennucci, S. Ransom, M. Roberts, and J. Hessels, Nature **467**, 1081 (2010), arXiv:1010.5788 [astro-ph.HE].
- [17] J. Antoniadis, P. C. Freire, N. Wex, T. M. Tauris, R. S. Lynch, M. H. van Kerkwijk, M. Kramer, C. Bassa, V. S. Dhillon, T. Driebe, J. W. T. Hessels, V. M. Kaspi, V. I. Kondratiev, N. Langer, T. R. Marsh, M. A. McLaughlin, T. T. Pennucci, S. M. Ransom, I. H. Stairs, J. van Leeuwen, J. P. W. Verbiest, and D. G. Whelan, Science **340**, 6131 (2013), arXiv:1304.6875 [astro-ph.HE].
- [18] F. Özel, D. Psaltis, S. Ransom, P. Demorest, and M. Alford, Astrophys.J. **724**, L199 (2010), arXiv:1010.5790 [astro-ph.HE].
- [19] S. Weissenborn, I. Sagert, G. Pagliara, M. Hempel, and J. Schaffner-Bielich, Astrophys.J. **740**, L14 (2011), arXiv:1102.2869 [astro-ph.HE].
- [20] E. S. Fraga, A. Kurkela, and A. Vuorinen, Astrophys. J. Lett. **781**, L25 (2014), arXiv:1311.5154 [nucl-th].
- [21] C. Ratti, M. A. Thaler, and W. Weise, Phys. Rev. **D73**, 014019 (2006), arXiv:hep-ph/0506234.
- [22] B.-J. Schaefer, J. M. Pawłowski, and J. Wambach, Phys.Rev. **D76**, 074023 (2007), arXiv:0704.3234 [hep-ph].
- [23] L. M. Haas, R. Stiele, J. Braun, J. M. Pawłowski, and J. Schaffner-Bielich, Phys.Rev. **D87**, 076004 (2013), arXiv:1302.1993 [hep-ph].
- [24] T. K. Herbst, M. Mitter, J. M. Pawłowski, B.-J. Schaefer, and R. Stiele, Phys.Lett. **B731**, 248 (2014), arXiv:1308.3621 [hep-ph].
- [25] D. Blaschke, T. Klähn, R. Lastowiecki, and F. Sandin, J. Phys. G **37**, 094063 (2010), arXiv:1002.1299 [nucl-th].
- [26] L. Bonanno and A. Sedrakian, Astron.Astrophys. **539**, A16 (2012), arXiv:1108.0559 [astro-ph.SR].
- [27] K. Masuda, T. Hatsuda, and T. Takatsuka, Prog. Theor. Exp. Phys. **2013**, 073D01 (2013), arXiv:1212.6803 [nucl-th].
- [28] K. Masuda, T. Hatsuda, and T. Takatsuka, Astrophys. J. **764**, 12 (2013), arXiv:1205.3621 [nucl-th].
- [29] M. Orsaria, H. Rodrigues, F. Weber, and G. Contrera, Phys.Rev. **D87**, 023001 (2013), arXiv:1212.4213 [astro-ph.SR].
- [30] M. Orsaria, H. Rodrigues, F. Weber, and G. Contrera, Phys.Rev. **C89**, 015806 (2014), arXiv:1308.1657 [nucl-th].
- [31] S. Benic, Eur.Phys.J. **A50**, 111 (2014), arXiv:1401.5380 [nucl-th].
- [32] N. Yasutake, R. Lastowiecki, S. Benic, D. Blaschke, T. Maruyama, *et al.*, Phys.Rev. **C89**, 065803 (2014), arXiv:1403.7492 [astro-ph.HE].
- [33] S. Benic, D. Blaschke, D. E. Alvarez-Castillo, T. Fischer, and S. Typel, Astron.Astrophys. **577**, A40 (2015), arXiv:1411.2856 [astro-ph.HE].
- [34] T. Klähn and T. Fischer, (2015), arXiv:1503.07442 [nucl-th].
- [35] H. Chen, M. Baldo, G. Burgio, and H.-J. Schulze, Phys.Rev. **D84**, 105023 (2011), arXiv:1107.2497 [nucl-th].
- [36] H. Chen, J.-B. Wei, M. Baldo, G. Burgio, and H.-J. Schulze, Phys.Rev. **D91**, 105002 (2015), arXiv:1503.02795 [nucl-th].
- [37] J. T. Lenaghan, D. H. Rischke, and J. Schaffner-Bielich, Phys. Rev. D **62**, 085008 (2000), arXiv:nucl-th/0004006.
- [38] T. Beisitzer, R. Stiele, and J. Schaffner-Bielich, Phys.Rev. **D90**, 085001 (2014), arXiv:1403.8011 [nucl-th].
- [39] B.-J. Schaefer and M. Wagner, Phys. Rev. **D79**, 014018 (2009), arXiv:0808.1491 [hep-ph].
- [40] For an extension considering σ_u and σ_d separately, see [56].
- [41] K. Schertler, C. Greiner, J. Schaffner-Bielich, and M. H. Thoma, Nucl. Phys. **A677**, 463 (2000), astro-ph/0001467.
- [42] G. Pagliara and J. Schaffner-Bielich, Phys. Rev. D **77**, 063004 (2008), arXiv:0711.1119 [astro-ph].
- [43] D. Parganlija, F. Giacosa, and D. H. Rischke, Phys.Rev. **D82**, 054024 (2010), arXiv:1003.4934 [hep-ph].
- [44] V. Koch, Int. J. Mod. Phys. **E6**, 203 (1997), nucl-th/9706075.
- [45] N. K. Glendenning and C. Kettner, Astron.Astrophys. **353**, L9 (2000), arXiv:astro-ph/9807155 [astro-ph].
- [46] M. Hanauske and W. Greiner, Gen.Rel.Grav. **33**, 739 (2001).
- [47] D. Alvarez-Castillo and D. Blaschke, (2013), arXiv:1304.7758 [astro-ph.HE].
- [48] M. G. Alford, S. Han, and M. Prakash, JPS Conf.Proc. **1**, 013041 (2014).
- [49] M. G. Alford, G. Burgio, S. Han, G. Taranto, and D. Zappal, (2015), arXiv:1501.07902 [nucl-th].
- [50] S. Banik and D. Bandyopadhyay, Phys.Rev. **D67**, 123003 (2003), arXiv:astro-ph/0212340 [astro-ph].
- [51] D. Blaschke and D. E. Alvarez-Castillo, (2015), arXiv:1503.03834 [astro-ph.HE].
- [52] A. Zacchi, M. Hanauske, and J. Schaffner-Bielich, (2015 - in preparation).
- [53] E. Farhi and R. L. Jaffe, Phys. Rev. D **30**, 2379 (1984).
- [54] J. Coelho, C. Lenzi, M. Malheiro, J. Marinho, R.M., C. Providencia, and M. Fiolhais, Nucl.Phys.Proc.Suppl. **199**, 325 (2010), arXiv:1001.1313 [nucl-th].
- [55] J. Torres and D. Menezes, Europhys.Lett. **101**, 42003 (2013), arXiv:1210.2350 [nucl-th].
- [56] R. Stiele, E. S. Fraga, and J. Schaffner-Bielich, Phys.Lett. **B729**, 72 (2014), arXiv:1307.2851 [hep-ph].